Int. J. Heat Mass Transfer. Vol. 18, pp. 1351–1360. Pergamon Press 1975. Printed in Great Britain

FLOW AND HEAT TRANSFER IN CURVED WALL JETS ON CIRCULAR SURFACES

H. MIYAZAKI and E. M. SPARROW
Department of Mechanical Engineering, University of Minnesota,
Minneapolis, Minnesota 55455, U.S.A.

(*Received* 11 *November* 1974 *and in revised form* 18 *February* 1975)

Abstract—Consideration is given to curved wall jets (i.e. flow along a wall which is curved in the streamwise direction) and, in particular, to flow along either a convex or a concave circular surface. The laminar flow and heat-transfer characteristics are investigated by making use of the method of inner and outer expansions. The Navier–Stokes and energy equations are expanded in series, with $1/\sqrt{Re}$ as the expansion parameter. The first-order equations are identical to the conventional boundary-layer equations, whereas the second-order equations are corrections for curvature and displacement effects. The latter equations were solved by a difference-differential method, with $Pr = 0{\cdot}72$ for the energy equation. The second-order correction increases the wall shear, the extent of the increase being greater for flow over a concave surface than for flow over a convex surface. On the other hand, the second-order correction either increases or decreases the Nusselt number, depending on whether the surface is convex or concave. The Coanda effect, whereby an induced transverse pressure difference inhibits flow separation, was demonstrated by the analysis.

NOMENCLATURE

C_f, local friction factor;
e_2, temperature variable, $\theta^{\frac{1}{2}}t_2$;
f_1, reduced stream function, equation (19);
h, local heat-transfer coefficient;
k, thermal conductivity;
N, stretched dimensionless normal coordinate, $n\sqrt{Re}$;
Nu, local Nusselt number $h\bar{r}/k$;
$\bar{n}$, $\bar{s}$, curvilinear coordinates;
n, s, dimensionless curvilinear coordinates, $\bar{n}/\bar{r}$, $\bar{s}/\bar{r}$;
P, dimensionless pressure for outer expansion;
Pr, Prandtl number;
$\bar{p}$, pressure;
p, dimensionless pressure for inner expansion, $(\bar{p}-\bar{p}_\infty)/\rho\bar{u}_r^2$;
Re, Reynolds number, $\bar{r}\bar{u}_r/\nu$;
$\bar{r}$, radius of circle;
r, dimensionless polar coordinate;
T, dimensionless temperature for outer expansion;
$\bar{t}$, temperature;
t, dimensionless temperature for inner expansion, $(\bar{t}-\bar{t}_w)/(\bar{t}_\infty-\bar{t}_w)$;
U, V, dimensionless velocity components for outer expansion;
$\bar{u}$, $\bar{v}$, velocity components;
u, v, dimensionless velocity components for inner expansion, $\bar{u}/\bar{u}_r$, $\bar{v}/\bar{u}_r$;
$\bar{u}_r$, reference velocity.

Greek symbols

α, thermal diffusivity;
η, similarity variable, equation (17);
θ, angular position coordinate;
$\bar{\kappa}$, curvature;
κ, dimensionless curvature, $\bar{r}\bar{\kappa}$;
ν, kinematic viscosity;
ρ, density;
τ, wall shear stress;
Ψ, dimensionless stream function for outer expansion;
ψ, dimensionless stream function for inner expansion.

Subscripts

1, first-order functions;
2, second-order functions;
∞, ambient;
w, wall.

Superscript

derivative with respect to η.

INTRODUCTION

A WALL jet is a fluid stream which is bounded on one side by a solid wall and on the other side by an otherwise quiescent fluid environment with which it can freely mix. One of the situations where a wall jet is encountered is on a surface on which a free jet has impinged. The wall jet is created by the impinging fluid which, after turning, flows along the surface. A wall jet may also be created by fluid directed tangentially along a surface by an injection slot. Among heat-transfer applications, wall jets are encountered in the drying of textiles and paper, tempering of glass, cooling of turbine blades, etc.

A two-dimensional wall jet flow on a flat surface may be termed a plane wall jet, whereas the designation *curved wall jet* may be employed to describe a two-dimensional wall jet flowing along a bounding wall

which is curved in the streamwise direction. In addition to heat-transfer applications, the curved wall jet is also of interest in aeronautical applications such as boundary-layer control and circulation control of airfoils. The present paper is concerned with laminar flow and heat transfer in curved wall jets along convex and concave circular surfaces.

The first analysis of a laminar wall jet flow was performed by Glauert [1], who treated the plane case using a conventional boundary-layer model (i.e. displacement effects due to the boundary layer were not included). A similarity solution was obtained in which a key parameter is the flux of external momentum. Although this quantity is an invariant for the Glauert problem, its numerical value cannot be determined from the similarity solution itself and, therefore, the solution is incomplete. This indeterminacy arises from the suppression of the boundary condition at the origin of the wall jet. A correction of Glauert's solution to account for the boundary-layer displacement effect was obtained by Plotkin [2].

There has been some study of the fluid flow aspects of curved laminar wall jets, but not of the heat transfer. Wygnanski and Champagne [3] simplified the Navier–Stokes equations by assuming that the boundary-layer thickness is small compared with the radius of curvature of the surface and that the variation of the latter along the surface is of order unity. They found a similarity solution for the special case in which the radius of curvature is proportional to the $\frac{3}{4}$ power of the arc length. The same similarity solution was independently obtained by Lindow and Greber [4].

More recently, Plotkin [5] solved the curved wall jet problem for flow along a specific parabolic surface using a truncated series in which the first term is Glauert's solution and the second term is a correction for curvature and for displacement effects. The solution contains an unknown characteristic velocity which was evaluated in terms of Glauert's flux of external momentum. Unfortunately, the latter quantity is not an invariant throughout the flow field for Plotkin's problem, so that its use in evaluating a constant reference velocity leads to an inconsistency. Clark and Watson [6] also used a truncated series to study the curved wall jet and applied their analytical method to flow along a parabolic surface. Their characteristic velocity was evaluated in the same way as was Plotkin's with the same inconsistency caused by the variability of the flux of external momentum.

The objective of the present study is to solve the flow and energy equations in order to obtain skin friction and heat-transfer characteristics of laminar wall jets flowing along convex and concave circular surfaces. The analysis is performed using Van Dyke's technique of inner and outer expansions [7]. The first-order solution is Glauert's similarity solution, and the second-order solution provides a correction for surface curvature and boundary-layer displacement. The partial differential equations for the second-order functions are solved by a difference–differential method. The heat-transfer solutions are for a Prandtl number of 0·72 (gases). To complete the solution, it is necessary to fix both the characteristic velocity and the effective origin of the wall jet.* A method is described whereby both quantities are determined with the aid of experimental information.

GOVERNING EQUATIONS

A schematic diagram showing coordinates and nomenclature for wall jet flow along a convex circular surface is presented in Fig. 1. The curvilinear co-

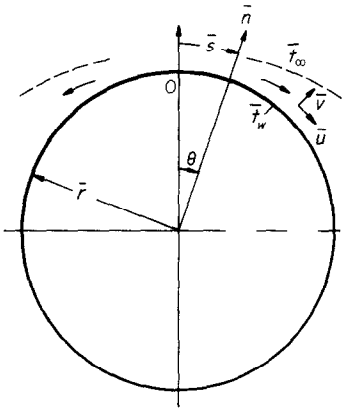

FIG. 1. Flow configuration and coordinate system.

ordinates $(\bar{s}, \bar{n})$ have their origin at 0; $\bar{s}$ is the arc length along the surface (i.e. $\bar{s} = \bar{r}\theta$) and $\bar{n}$ is the local outward normal. Consideration is given here to the symmetry case where the flow field is identical at all pairs of streamwise stations s and $-s$. The flow direction is indicated in the diagram. For the case of flow on the concave (i.e. inner) surface of the circle, the directions of $\bar{n}$ and $\bar{v}$ are reversed relative to those of Fig. 1.

For constant property laminar flows, the equations of mass, momentum, and energy conservation may be written in terms of curvilinear coordinates as [8]

$$\frac{\partial \bar{u}}{\partial \bar{s}} + \frac{\partial}{\partial \bar{n}}[(1+\bar{\kappa}\bar{n})\bar{v}] = 0, \tag{1}$$

$$\frac{1}{1+\bar{\kappa}\bar{n}}\bar{u}\frac{\partial \bar{u}}{\partial \bar{s}} + \bar{v}\frac{\partial \bar{u}}{\partial \bar{n}} + \frac{\bar{\kappa}}{1+\bar{\kappa}\bar{n}}\bar{u}\bar{v} = -\frac{1}{1+\bar{\kappa}\bar{n}}\frac{1}{\rho}\frac{\partial \bar{p}}{\partial \bar{s}} + \nu\left\{\frac{1}{(1+\bar{\kappa}\bar{n})^2}\frac{\partial^2 \bar{u}}{\partial \bar{s}^2} + \frac{\partial^2 \bar{u}}{\partial \bar{n}^2} + \frac{\bar{\kappa}}{1+\bar{\kappa}\bar{n}} \times \frac{\partial \bar{u}}{\partial \bar{n}} - \frac{\bar{\kappa}^2}{(1+\bar{\kappa}\bar{n})^2}\bar{u} + \frac{2\bar{\kappa}}{(1+\bar{\kappa}\bar{n})^2}\frac{\partial \bar{v}}{\partial \bar{s}}\right\}, \tag{2}$$

$$\frac{1}{1+\bar{\kappa}\bar{n}}\bar{u}\frac{\partial \bar{v}}{\partial \bar{s}} + \bar{v}\frac{\partial \bar{v}}{\partial \bar{n}} - \frac{\bar{\kappa}}{1+\bar{\kappa}\bar{n}}\bar{u}^2 = -\frac{1}{\rho}\frac{\partial \bar{p}}{\partial \bar{n}} + \nu\left\{\frac{1}{(1+\bar{\kappa}\bar{n})^2}\frac{\partial^2 \bar{v}}{\partial \bar{s}^2} + \frac{\partial^2 \bar{v}}{\partial \bar{n}^2} + \frac{\bar{\kappa}}{1+\bar{\kappa}\bar{n}}\frac{\partial \bar{v}}{\partial \bar{n}} - \frac{\bar{\kappa}^2}{(1+\bar{\kappa}\bar{n})^2}\bar{v} - \frac{2\bar{\kappa}}{(1+\bar{\kappa}\bar{n})^2}\frac{\partial \bar{u}}{\partial \bar{s}}\right\}, \tag{3}$$

* The need to fix the effective origin is common to all of the analyses cited in the foregoing, but the issue appears not to have been addressed therein.

$$\frac{1}{1+\bar{\kappa}\bar{n}}\bar{u}\frac{\partial \bar{t}}{\partial \bar{s}}+\bar{v}\frac{\partial \bar{t}}{\partial \bar{n}} = \alpha\left\{\frac{1}{(1+\bar{\kappa}\bar{n})^2}\frac{\partial^2 \bar{t}}{\partial \bar{s}^2}+\frac{\partial^2 \bar{t}}{\partial \bar{n}^2}+\frac{\bar{\kappa}}{1+\bar{\kappa}\bar{n}}\frac{\partial \bar{t}}{\partial \bar{n}}\right\}. \quad (4)$$

In the foregoing, the overbar identifies a dimensional quantity. The curvature $\bar{\kappa}$ is the reciprocal of the radius of the circle in the present problem.

To construct dimensionless quantities, the radius of the circle $\bar{r}$ is used as a length scale, and an as-yet unspecified reference velocity $\bar{u}_r$ is used as the velocity scale. Then, the dependent variables are

$$\bar{u}/\bar{u}_r,\ \bar{v}/\bar{u}_r,\ (\bar{t}-\bar{t}_w)/(\bar{t}_\infty-\bar{t}_w),\ (\bar{p}-\bar{p}_\infty)/\rho\bar{u}_r^2$$

and (5)

$$s=\bar{s}/\bar{r}=\theta,\ n=\bar{n}/\bar{r},\ \kappa=\bar{\kappa}\bar{r},\ Re=\bar{r}\bar{u}_r/\nu$$

where κ takes on values of ± 1 respectively for the convex and concave surfaces.

It is well known that the dimensionless thickness of the boundary layer is of order $1/\sqrt{Re}$. Accordingly, a new boundary-layer normal coordinate which is of order unity may be defined as $N=n\sqrt{Re}$. The transverse velocity within the boundary layer is also small and should be magnified in a similar manner. Once these scalings have been made, the conventional boundary-layer equations are obtained by letting Re become infinite with N fixed. However, when Re is only moderately large, as in the case in a laminar wall jet and, in addition, if the surface curvature is sufficiently large so that the boundary-layer thickness becomes comparable to the radius of curvature, the conventional boundary-layer equations are inadequate to describe the flow.

Van Dyke's method of inner and outer expansions [7] is used here to derive governing equations which are subsequently solved to obtain a better representation of the flow and heat transfer. The basis of the method is to expand both the inner (boundary layer) flow and the outer (inviscid) flow in series, with boundary conditions for the functions in the expansions being provided by a matching of the two flows.

Although the flow outside the boundary layer is inviscid, it is affected by the presence of the boundary layer. The first-order correction of the outer flow owing to this effect is of order $1/\sqrt{Re}$. Consequently, the outer expansions (i.e. for the inviscid flow) are expressible in dimensionless form as

$$\begin{aligned} U &= U_1+U_2/\sqrt{Re}+\ldots,\\ V &= V_1+V_2/\sqrt{Re}+\ldots,\\ P &= P_1+P_2/\sqrt{Re}+\ldots,\\ T &= T_1+T_2/\sqrt{Re}+\ldots,\\ \Psi &= \Psi_1+\Psi_2/\sqrt{Re}+\ldots. \end{aligned} \quad (6)$$

For the present problem, all of the functions in equation (6) with subscript one are zero, except T_1 which is unity. The stream function Ψ_2 obeys Laplace's equation, and U_2 and V_2 are obtained from Ψ_2 by differentiation. P_2 and T_2 are found to be zero in the present problem.

The velocity components, the pressure, and the temperature for the boundary-layer flow are also expanded in series

$$\begin{aligned} u &= u_1+u_2/\sqrt{Re}+\ldots\\ v &= v_1/\sqrt{Re}+v_2/Re+\ldots\\ p &= p_1+p_2/\sqrt{Re}+\ldots\\ t &= t_1+t_2/\sqrt{Re}+\ldots. \end{aligned} \quad (7)$$

It may be noted that the form of the expansion for v was chosen so that $v_1\sim u_1$, $v_2\sim u_2$.

Substitution of equations (7) into the dimensionless counterparts of (1)–(4) and collection of terms with similar powers of Re leads to the governing equations for the successive inner approximations. The first-order equations are, with $N=n\sqrt{Re}$,

$$\frac{\partial u_1}{\partial s}+\frac{\partial v_1}{\partial N}=0, \quad (8)$$

$$u_1\frac{\partial u_1}{\partial s}+v_1\frac{\partial u_1}{\partial N}=-\frac{\partial p_1}{\partial s}+\frac{\partial^2 u_1}{\partial N^2}, \quad (9)$$

$$0=-\frac{\partial p_1}{\partial N}, \quad (10)$$

$$u_1\frac{\partial t_1}{\partial s}+v_1\frac{\partial t_1}{\partial N}=\frac{1}{Pr}\frac{\partial^2 t_1}{\partial N^2}. \quad (11)$$

The second-order equations are given by

$$\frac{\partial u_2}{\partial s}+\frac{\partial}{\partial N}(v_2+\kappa N v_1)=0, \quad (12)$$

$$\begin{aligned} u_1\frac{\partial u_2}{\partial s}+u_2\frac{\partial u_1}{\partial s}+v_1\frac{\partial u_2}{\partial N}+v_2\frac{\partial u_1}{\partial N} &= -\frac{\partial p_2}{\partial s}+\frac{\partial^2 u_2}{\partial N^2}+\kappa N\frac{\partial p_1}{\partial s}\\ &\quad +\kappa N u_1\frac{\partial u_1}{\partial s}-\kappa u_1 v_1+\kappa\frac{\partial u_1}{\partial N}, \end{aligned} \quad (13)$$

$$\kappa u_1^2=\frac{\partial p_2}{\partial N}+\kappa N\frac{\partial p_1}{\partial N}, \quad (14)$$

$$\begin{aligned} u_1\frac{\partial t_2}{\partial s}+u_2\frac{\partial t_1}{\partial s}+v_1\frac{\partial t_2}{\partial N}+v_2\frac{\partial t_1}{\partial N} &= \frac{1}{Pr}\frac{\partial^2 t_2}{\partial N^2}+\kappa N u_1\frac{\partial t_1}{\partial s}+\frac{\kappa}{Pr}\frac{\partial t_1}{\partial N}. \end{aligned} \quad (15)$$

The boundary conditions at the wall for the outer expansions and at the edge of the boundary layer for the inner expansions are found by matching the inner and outer solutions.

SOLUTIONS OF THE MOMENTUM EQUATIONS

First-order inner solution

The governing equations for the first-order inner solution are expressed by (8)–(10). The asymptotic boundary conditions at the edge of the boundary layer, which result from the inner–outer matching, are that $u_1\to U_1(\theta,0)$ and $p_1\to P_1(\theta,0)$. Since both U_1 and P_1 are zero, it follows that $u_1\to 0$ as $N\to\infty$ and that $p_1=0$ everywhere in accordance with equation (10).

Then, the complete statement of the boundary conditions for equations (8) and (9) is

$$u_1 = v_1 = 0 \text{ at } N = 0; \quad u_1 \to 0 \text{ as } N \to \infty. \quad (16)$$

Equations (8) and (9) with the boundary conditions (16) were solved by Glauert [1] using a similarity transformation. By the introduction of a similarity variable

$$\eta = (\tfrac{1}{4})\theta^{-\frac{1}{4}}N \quad (17)$$

the momentum equation reduces to

$$f_1''' + f_1 f_1'' + 2(f_1')^2 = 0$$
$$f_1(0) = f_1'(0) = 0, \quad \text{and} \quad f_1'(\eta) \to 0 \text{ as } \eta \to \infty \quad (18)$$

where f_1 is defined by

$$\psi_1(\theta, N) = \theta^{\frac{1}{4}} f_1(\eta). \quad (19)$$

The solution to equation (18) is obtained in closed form as

$$\eta = \frac{1}{2}\ln\left\{\frac{1+f_1^{\frac{1}{4}}+f_1}{(1-\sqrt{f_1})^2}\right\} + 3^{\frac{1}{4}}\tan^{-1}\left(\frac{(3f_1)^{\frac{1}{4}}}{2+\sqrt{f_1}}\right). \quad (20)$$

From this, the friction factor associated with the first-order flow is

$$C_{f1} = \tau_{1w}/(\tfrac{1}{2}\rho\bar{u}_r^2) = \theta^{-\frac{1}{4}} f_1''(0)/(8\sqrt{Re}), \quad (21)$$

where $f_1''(0) = \frac{2}{9}$.

Second-order outer solution

As already noted, $P_2 = 0$ and Ψ_2 is governed by Laplace's equation. The boundary condition for Ψ_2 at the wall follows from the inner–outer matching as [7]

$$\Psi_2(\theta, 0) = \lim_{N\to\infty}\left(\psi_1 - N\frac{\partial\psi_1}{\partial N}\right) = \theta^{\frac{1}{4}}. \quad (22)$$

Thus, as far as Ψ_2 is concerned, the first-order boundary-layer solution provides, via equation (22), a source of mass distributed along the surface. Since consideration is being given here to a symmetric flow, the boundary condition (22) is appropriately rewritten as

$$\Psi(\theta, 0) = \text{sgn}(\theta)|\theta|^{\frac{1}{4}}. \quad (23)$$

If consideration is first given to the concave case, the task is to solve

$$\frac{\partial^2\Psi_2}{\partial r^2} + \frac{1}{r}\frac{\partial\Psi_2}{\partial r} + \frac{1}{r^2}\frac{\partial\Psi_2}{\partial\theta^2} = 0 \quad \text{for} \quad r < 1, \quad (24)$$

$$\Psi_2 = \text{sgn}(\theta)|\theta|^{\frac{1}{4}} \quad \text{at} \quad r = 1. \quad (25)$$

The solution is given by Poisson's integral formula

$$\Psi_2(\theta, r) = \frac{1-r^2}{2\pi}\int_{-\pi}^{\pi}\frac{\text{sgn}(\phi)|\phi|^{\frac{1}{4}}}{1+r^2-2r\cos(\theta-\phi)}\,d\phi, \quad (26)$$

or, transforming from r to n with $r = (1-n)$,

$$\Psi_2(\theta, n) = \frac{1-(1-n)^2}{2\pi}\int_{-\pi}^{\pi}\frac{\text{sgn}(\phi)|\phi|^{\frac{1}{4}}}{1+(1-n)^2-2(1-n)\cos(\theta-\phi)}. \quad (27)$$

The velocity U_2 at the wall, which is needed as a boundary condition for the forthcoming second-order inner solution, is calculated from

$$U_2(\theta, 0) = \lim_{n\to 0}\frac{\partial\Psi_2}{\partial n}. \quad (28)$$

Ψ_2 has a singular point at $n = 0$ and $\phi = \theta$, so that equation (27) has to be modified to facilitate the numerical evaluation of equation (28). If the stream function on the surface were constant and equal to unity, the solution would then be $\Psi_2 = 1$, that is, equation (27) would become

$$1 = \frac{1-(1-n)^2}{2\pi} \times \int_{-\pi}^{\pi}\frac{1}{1+(1-n)^2-2(1-n)\cos(\theta-\phi)}\,d\phi. \quad (29)$$

Multiplying both sides of equation (29) by $\Psi_2(\theta, 0) = \text{sgn}(\theta)|\theta|^{\frac{1}{4}}$ and subtracting it from equation (27), one obtains

$$\Psi_2(\theta, n) - \Psi_2(\theta, 0) = \frac{1-(1-n)^2}{2\pi}\int_{-\pi}^{\pi}\frac{\text{sgn}(\phi)|\phi|^{\frac{1}{4}} - \text{sgn}(\theta)|\theta|^{\frac{1}{4}}}{1+(1-n)^2-2(1-n)\cos(\theta-\phi)}\,d\phi. \quad (30)$$

Then, $U_2(\theta, 0)$ is given by

$$U_2(\theta, 0) = \lim_{n\to 0}\frac{\Psi_2(\theta, n) - \Psi_2(\theta, 0)}{n} = \frac{1}{2\pi}\int_{-\pi}^{\pi}\frac{\text{sgn}(\phi)|\phi|^{\frac{1}{4}} - \text{sgn}(\theta)|\theta|^{\frac{1}{4}}}{1-\cos(\theta-\phi)}\,d\phi. \quad (31)$$

For flow along a convex surface, Ψ_2 can be solved for by an inversion which transforms the outside of the circle into the inside. From these operations, it is found that $U_2(\theta, 0)$ is expressed by exactly the same equation as (31).

Since $\phi = \theta$ is a singular point, the interval of integration should be divided into three regions, i.e. $-\pi$ to $(\theta-\varepsilon)$, $(\theta-\varepsilon)$ to $(\theta+\varepsilon)$, and $(\theta+\varepsilon)$ to π, and the numerical integration should be performed separately in each region. It is easy to show that the second integral approaches zero as ε tends to zero.

Second-order inner solution

Since $p_1 = 0$, all the terms in equations (13) and (14) which contain p_1 vanish. The pressure p_2 is found from equation (14) with the boundary condition $p_2 \to P_2 = 0$ as $N \to \infty$.

$$p_2 = -\kappa\int_N^{\infty} u_1^2\,dN = -\frac{1}{4}\kappa\theta^{-\frac{1}{4}}(f_1'' + f_1 f_1'). \quad (32)$$

In particular, the pressure at the wall is

$$p_2(\theta, 0) = -\frac{1}{4}\kappa f_1''(0)\theta^{-\frac{1}{4}} = -\frac{1}{18}\kappa\theta^{-\frac{1}{4}}. \quad (33)$$

To initiate the solution of the momentum equation (13), a stream function ψ_2 is introduced to satisfy equation (12).

$$u_2 = \frac{\partial\psi_2}{\partial N}, \quad v_2 + \kappa N v_1 = -\frac{\partial\psi_2}{\partial\theta}, \quad (34)$$

or $$u_2 = \frac{1}{4}\theta^{-\frac{1}{2}}\frac{\partial\psi_2}{\partial\eta},$$

$$v_2 = \kappa\eta(f_1 - 3\eta f_1') - \frac{\partial\psi_2}{\partial\theta} + \frac{3}{4}\theta^{-1}\eta\frac{\partial\psi_2}{\partial\eta}, \quad (35)$$

where the last term in the v_2 equation of (35) results from the change of variable from N to η. Substitution of equations (32) and (35) into (13) yields

$$\frac{\partial^3\psi_2}{\partial\eta^3} + f_1\frac{\partial^2\psi_2}{\partial\eta^2} + 5f_1'\frac{\partial\psi_2}{\partial\eta} - 4\theta\left(f_1'\frac{\partial^2\psi_2}{\partial\theta\partial\eta} - f_1''\frac{\partial\psi_2}{\partial\theta}\right) = -4\kappa\theta\eta f_1''', \quad (36)$$

which is subject to the boundary conditions

$$\psi_2 = \partial\psi_2/\partial\eta = 0 \quad \text{at} \quad \eta = 0,$$
$$\partial\psi_2/\partial\eta \to 4\theta^{\frac{1}{2}}U_2(\theta, 0) \quad \text{as} \quad \eta \to \infty. \quad (37)$$

The last boundary condition in (37) results from the matching condition $u_2 \to U_2(\theta, 0)$ as $N \to \infty$.

At $\theta = 0$, equations (36) and (37) reduce to

$$\frac{\partial^3\psi_2}{\partial\eta^3} + f_1\frac{\partial^2\psi_2}{\partial\eta^2} + 5f_1'\frac{\partial\psi_2}{\partial\eta} = 0,$$

$$\psi_2 = \frac{\partial\psi_2}{\partial\eta} = 0 \quad \text{at} \quad \eta = 0, \quad (38)$$

$$\frac{\partial\psi_2}{\partial\eta} \to \lim_{\theta\to 0} 4\theta^{\frac{1}{2}}U_2(\theta, 0) = -(\sqrt{2}+1) \text{ as } \eta \to \infty.$$

Inasmuch as there are no θ derivatives in the differential equation for ψ_2, it can be treated as an ordinary differential equation. The needed input information for f_1 and its derivatives is available in implicit form [see equation (20)], but this is inconvenient for an accurate solution of equation (38). Instead, equations (18) and (38) were solved simultaneously by the Runge–Kutta method to an accuracy of eight significant figures.

The solution of equation (36) for $\theta > 0$ was carried out by a difference–differential method. At the first step, the θ derivatives were approximated by a one-sided forward difference, whereas for subsequent steps a three-point difference was employed. The step size $\Delta\theta$ was $\pi/40$. The quasi-ordinary differential equation which resulted at each step was solved by the Runge–Kutta method. The input values of f_1 and its derivatives needed for the solutions were read from the computer memory where they had been placed subsequent to solution of equation (18). The step size $\Delta\eta$ and maximum η were 0·05 and 25, respectively. Verification runs in which $\Delta\eta$ and η_{max} were varied indicated five significant figure accuracies for the friction factor.

The friction factor associated with the second-order flow is given by

$$C_{f2} = \tau_{2w}\Big/\left(\frac{1}{2}\rho\bar{u}_r^2\right) = \left(\frac{\partial^2\psi_2}{\partial\eta^2}\right)_{\eta=0}\theta^{-\frac{1}{2}}/(8Re). \quad (39)$$

The total friction factor is, therefore,

$$C_f = C_{f1} + C_{f2}$$
$$= \theta^{-\frac{1}{2}}/(36\sqrt{Re}) + \left(\frac{\partial^2\psi_2}{\partial\eta^2}\right)_{\eta=0}\theta^{-\frac{1}{2}}/(8Re), \quad (40)$$

or $$C_f/C_{f1} = 1 + \frac{9}{2}\left(\frac{\partial^2\psi_2}{\partial\eta^2}\right)_{\eta=0}\theta^{-\frac{1}{2}}/\sqrt{Re}. \quad (41)$$

SOLUTIONS OF THE ENERGY EQUATIONS

First-order inner solution

The energy equation (11) for the first-order inner solution can be transformed into an ordinary differential equation by the use of the similarity variable η.

$$t_1'' + Prf_1t' = 0. \quad (42)$$

The matching of inner and outer solutions requires that $t_1 \to T_1(\theta, 0)$ as $\eta \to \infty$, and since $T_1 = 1$ it follows that $t_1 \to 1$. The boundary conditions can then be stated as

$$t_1 = 0 \text{ at } \eta = 0; \quad t_1 \to 1 \text{ as } \eta \to \infty. \quad (43)$$

The solution of equations (42)–(43) can be written in a closed-form expression involving a double integral which must be evaluated numerically. It was found that greater accuracy could be attained by a direct numerical solution of equation (42) using the Runge–Kutta method. Once the solution has been performed, the Nusselt number for the first-order solution can be evaluated from

$$Nu_1 = h_1\bar{r}/k = (\tfrac{1}{4})\theta^{-\frac{1}{2}}(Re)^{\frac{1}{2}}t_1'(0). \quad (44)$$

The quantity $t_1'(0)$ is a function of Prandtl number and is equal to 0·28623 for $Pr = 0{\cdot}72$.

Second-order inner solution

The energy equation for the second-order inner solution is expressed by equation (15) which, after transformation into (θ, η) coordinates, becomes

$$\frac{1}{Pr}\frac{\partial^2t_2}{\partial\eta^2} + f_1\frac{\partial t_2}{\partial\eta} - 4\theta f_1'\frac{\partial t_2}{\partial\theta} = -4\theta^{\frac{1}{2}}\left\{\kappa\left(\frac{1}{Pr} - \eta f_1\right) + \frac{\partial\psi_2}{\partial\theta}\right\}t_1'. \quad (45)$$

Inasmuch as the outer solution yields $T_2 = 0$, the boundary conditions for t_2 are

$$t_2 = 0 \text{ at } \eta = 0; \quad t_2 \to 0 \text{ as } \eta \to \infty. \quad (46)$$

Next, a change of variable $e_2 = \theta^{\frac{1}{2}}t_2$ was introduced with the expectation that the derivative $e_2'(0)$ would have a "nicer" θ dependence than the derivative $t_2'(0)$. These quantities enter into the evaluation of the Nusselt number. From an examination of equation (45) in the neighborhood of the wall, it can be conjectured that $\theta^{\frac{1}{2}}t_2 \sim \theta$, so that $e_2'(0)$ should be nearly linear in θ. After transformation, equation (45) becomes

$$\frac{1}{Pr}\frac{\partial^2e_2}{\partial\eta^2} + f_1\frac{\partial e_2}{\partial\eta} - 4\theta f_1'\frac{\partial e_2}{\partial\theta} + f_1'e_2 = -4\theta\left\{\kappa\left(\frac{1}{Pr} - \eta f_1\right) + \frac{\partial\psi_2}{\partial\theta}\right\}t_1', \quad (47)$$

with boundary conditions for e_2 that are identical to those for t_2 [equation (46)].

Equation (47) was solved by the same difference–differential method that was employed to solve equation (36). The calculations were performed for a Prandtl number of 0·72. At $\theta = 0$, it can be shown that $e_2 = 0$.

The Nusselt number can then be evaluated as

$$Nu_2 = h_2\bar{r}/k = (\tfrac{1}{4})\theta^{-1}(\partial e_2/\partial\eta)_{\eta=0}. \quad (48)$$

Then, by making use of equations (44) and (48), there follows

$$Nu = Nu_1 + Nu_2 = (\tfrac{1}{4})\theta^{-\frac{1}{2}}(Re)^{\frac{1}{2}}f_1'(0) + (\tfrac{1}{4})\theta^{-1}(\partial e_2/\partial\eta)_{\eta=0} \quad (49)$$

or

$$Nu/Nu_1 = 1 + \left\{\left(\frac{\partial e_2}{\partial\eta}\right)_{\eta=0}\Big/ f_1'(0)\right\}\theta^{-\frac{1}{2}}/(Re)^{\frac{1}{2}}. \quad (50)$$

RESULTS AND DISCUSSION

The free stream velocity induced by the first-order boundary-layer solution and imposed on the second-order boundary-layer flow is represented by $U_2(\theta, 0) = U_2(s, 0)$. As explained earlier, this quantity is obtained by solving the second-order outer flow. The results for $U_2(s, 0)$ are plotted in Fig. 2, where the solid and dashed lines correspond respectively to flow along a circular surface and to flow along a flat plate (plane wall jet). Also plotted for both surfaces is the quantity $4s^{\frac{3}{4}}U_2(s, 0)$, which is the boundary value of $\partial\psi_2/\partial\eta$ as $\eta \to \infty$. The plane wall jet results are from [6].

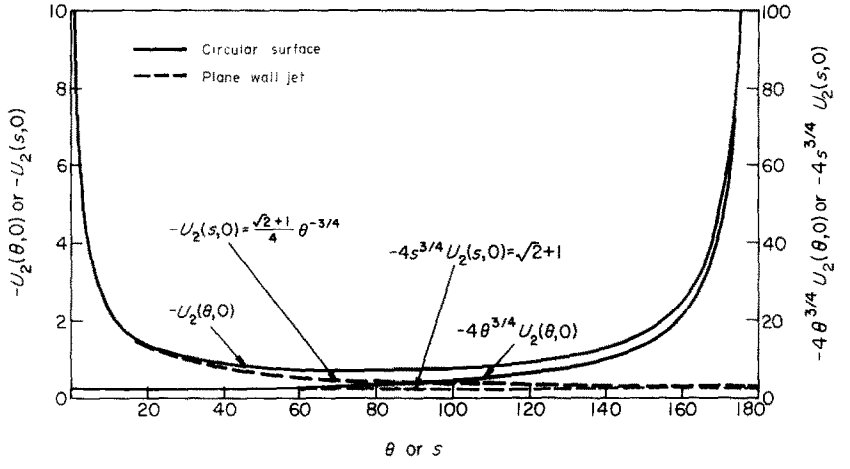

FIG. 2. Free stream velocity induced by the first-order boundary-layer flow.

Inspection of the figure reveals that $U_2(s, 0)$ is negative, that is, the direction of the induced free stream flow is opposite to that of the first-order boundary-layer flow. This behavior can be made plausible by considering the way in which $U_2(s, 0)$ is induced. The first-order boundary-layer flow entrains otherwise quiescent fluid from the environment, so that the transverse velocity at the edge of the boundary layer is negative. From the standpoint of the second-order outer flow, this is equivalent to the presence of a sink of mass distributed along the surface. Since the strength of the sink decreases with s (or θ), the induced flow is negative, i.e. $U_2(s, 0)$ is negative.

The just-discussed behavior is opposite to that encountered in the classical Blasius flow along a flat plate. In that case, the first-order boundary layer causes a positive normal velocity, which is equivalent to a distributed source of mass.

It might be expected that the circular surface would behave like a flat surface in the neighborhood of $\theta = s = 0$. This expectation is verified by the coincidence of the solid and dashed lines when θ and s are small. Since $U_2(s, 0) \sim s^{-\frac{3}{4}}$ for small values of s, it follows that $s^{\frac{3}{4}}U_2(s, 0)$ approaches a constant. It is also worth noting that $U_2(0, 0) = 0$, which is different from the limit $U_2 = -\infty$ as $s \to 0$.

Representative profiles of the streamwise velocity u_2 of the second-order boundary-layer solution are plotted in Fig. 3 as a function of the stretched normal coordinate N. The solid and dashed curves correspond respectively to flow along a convex and a concave surface. The results are for three streamwise stations, $\theta = 49{\cdot}5°$, $85{\cdot}5°$, and $139{\cdot}5°$.

It is especially interesting to note in the figure that u_2 is positive near the wall even though the free stream velocity is negative. Furthermore, at any streamwise location, the velocities and gradients in the near-wall region are larger for the concave surface than for the convex surface. With increasing downstream distance, the positive velocities appear to diminish.

That $u_2 > 0$ near the wall is an indication that the second-order boundary-layer flow in that region is more influenced by the inertia of the first-order boundary layer than by its own free stream velocity. However, as the downstream distance increases, the inertia contribution diminishes and, as a consequence, the positive velocities grow smaller.

To explain the higher u_2 values exhibited by the concave surface in the near-wall region, it is relevant to examine the curvature-dependent terms on the RHS of equation (13). These terms, taken together, represent a net force on the flow. By the use of equations (8), (9), and (32), it can be shown that

$$-(\partial p_2/\partial s) = \kappa u_1 v_1 - \kappa(\partial u_1/\partial N). \quad (51)$$

With this, the curvature-dependent terms on the right of equation (13) collapse to a single term, $\kappa u_1 N\partial u_1/\partial s$. In the near-wall region, this quantity is positive for a concave surface and negative for a convex surface. Therefore, for the former surface, the curvature terms

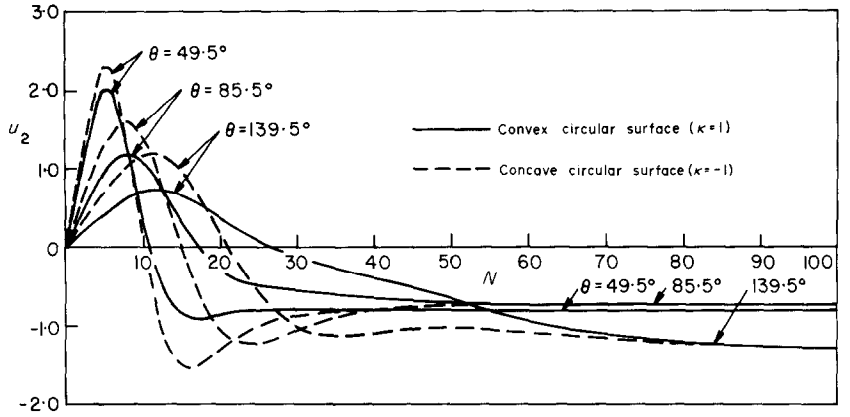

FIG. 3. Representative velocity profiles for the second-order boundary-layer flow.

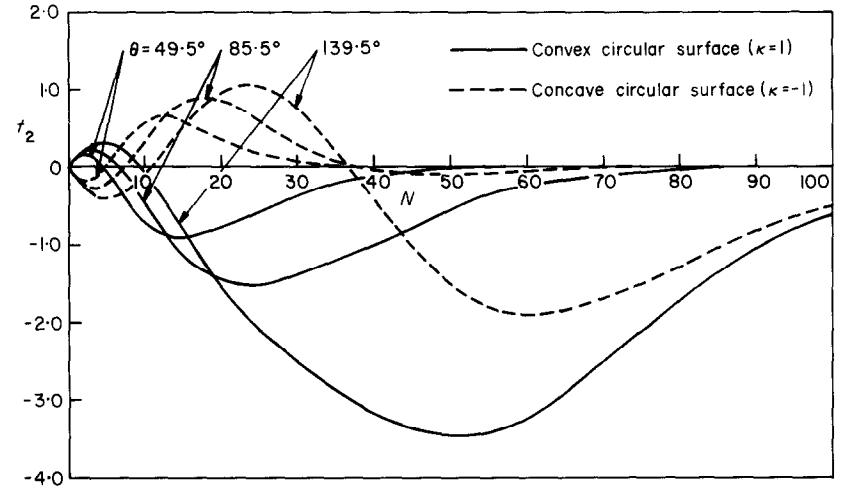

FIG. 4. Representative temperature profiles for the second-order boundary-layer flow, $Pr = 0{\cdot}72$.

tend to augment the velocities whereas the opposite effect is in force for the latter.

Figure 4 contains representative profiles of the second-order temperature t_2 which are plotted at the same streamwise locations as were the velocity profiles of Fig. 3. These results are for $Pr = 0{\cdot}72$. As before, the solid and dashed lines are for the convex and concave surfaces, respectively. It may be noted that in the near-wall region, the sign of t_2 and of its slope for the concave surface are just opposite to the corresponding sign for the convex surface. Also, for each surface, the gradient $\partial t_2/\partial N$ at $N = 0$ appears to be independent of streamwise location.

To examine the near-wall behavior, it is fruitful to consider the terms

$$\kappa u_1 N \partial t_1/\partial s + (\kappa/Pr)\partial t_1/\partial N \tag{52}$$

that play the role of heat sources or sinks on the RHS of the t_2 energy equation (15). Near the wall, the signs of the two terms are opposite to each other, but the second term is predominant and is positive (i.e. a source) when the surface is convex and negative (i.e. a sink) when the surface is concave. Furthermore, the convection terms can be neglected near the wall. It then follows from equation (15) that the conduction term $\partial^2 t_2/\partial N^2$ carries heat to the wall in the case of a convex surface and away from the wall in the case of a concave surface. Therefore, the opposite orientations of the t_2 profiles are as they should be.

With respect to the θ-independence of $(\partial t_2/\partial N)_{N=0}$, it is useful to note that

$$(\partial t_2/\partial N)_{N=0} \sim (1/\theta)(\partial e_2/\partial \eta)_{\eta=0} \tag{53}$$

from which it follows that $(\partial e_2/\partial \eta)_{\eta=0} \sim \theta$ when $(\partial t_2/\partial N)_{N=0}$ is independent of θ. Therefore, the numerical solutions verify a conjecture based on the a priori examination of (45).

The pressure distribution along the wall from the second-order inner solution is presented in Fig. 5. Since the first-order inner solution gives $p_1 = 0$, it follows from equation (7) that $p = p_2/\sqrt{Re}$. Actually, it is the magnitude of $(p_2)_{\eta=0}$ that is plotted in the figure. According to equation (33), $(p_2)_{\eta=0} < 0$ for a convex surface and > 0 for a concave surface. The pressure varies with $\theta^{-\frac{1}{2}}$ along the wall.

It is especially interesting to note that for the convex surface, the pressure at the wall is less than that of the free stream. The effect of this pressure defect is to press the flow against the wall, thereby delaying separation. This behavior is often referred to as the Coanda Effect.

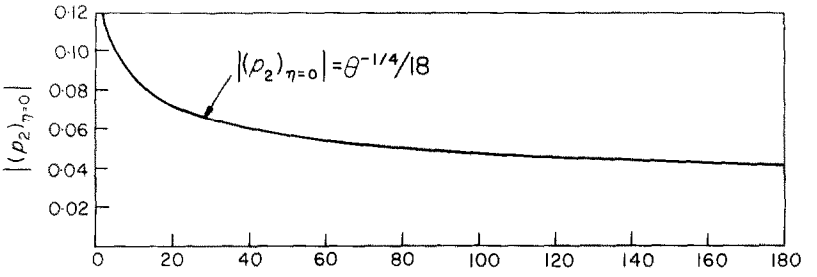

FIG. 5. Pressure distribution on the surface.

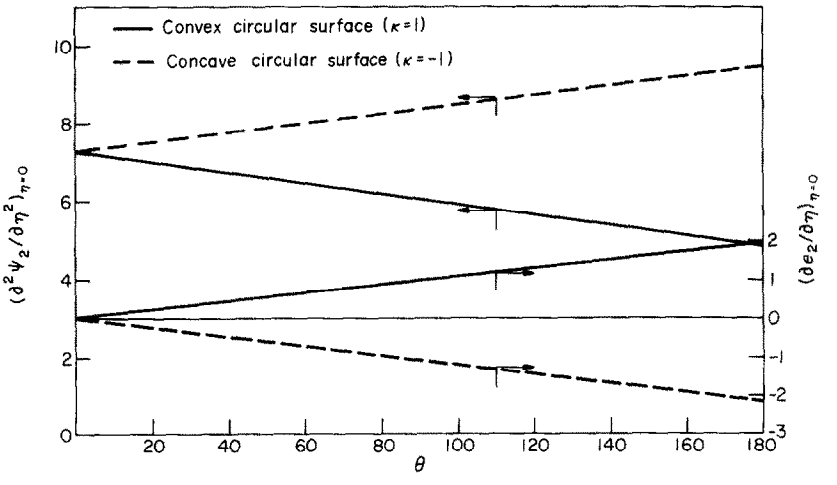

FIG. 6. Derivatives of stream function and temperature at the surface, respectively related to friction factor and Nusselt number. The temperature derivative results are for $Pr = 0{\cdot}72$.

In the present analysis, the wall jet never separates from the bounding surface.

The quantities $(\partial^2\psi_2/\partial\eta^2)_{\eta=0}$ and $(\partial e_2/\partial\eta)_{\eta=0}$, which are respectively related to C_{f2} and Nu_2, are plotted in Fig. 6 as a function of the streamwise position coordinate θ. Both of these quantities vary almost linearly with θ. The former begins with a positive value at $\theta = 0$ and either increases or decreases according to whether the wall is concave or convex. On the other hand, the latter takes on a zero value at $\theta = 0$ and displays a variation with θ just opposite to the aforementioned. The $(\partial e_2/\partial\eta)_{\eta=0}$ results are for $Pr = 0{\cdot}72$.

Straight lines fitted through the results can be represented as

$$\begin{aligned}(\partial^2\psi_2/\partial\eta^2)_{\eta=0} &= 7{\cdot}243-0{\cdot}752\theta \\ &\text{with error } <2{\cdot}0 \text{ per cent,} \\ (\partial e_2/\partial\eta)_{\eta=0} &= 0{\cdot}626\theta \\ &\text{with error } <3{\cdot}7 \text{ per cent,}\end{aligned} \tag{54}$$

for the convex circular surface, and

$$\begin{aligned}(\partial^2\psi_2/\partial\eta^2)_{\eta=0} &= 7{\cdot}243+0{\cdot}720\theta \\ &\text{with error } <2{\cdot}1 \text{ per cent,} \\ (\partial e_2/\partial\eta)_{\eta=0} &= -0{\cdot}673\theta \\ &\text{with error } <3{\cdot}4 \text{ per cent,}\end{aligned} \tag{55}$$

for the concave circular surface.

The corresponding formulas for the friction factors and the Nusselt numbers then become

$$\begin{aligned}C_{f_2} &= (0{\cdot}905-0{\cdot}0940\theta)\theta^{-\frac{1}{2}}/Re, \\ C_f &= \theta^{-\frac{1}{2}}/(36\sqrt{Re})+(0{\cdot}905-0{\cdot}0940\theta)\theta^{-\frac{1}{2}}/Re, \\ C_f/C_{f_1} &= 1+(32{\cdot}59-3{\cdot}38\theta)\theta^{-\frac{1}{2}}/\sqrt{Re},\end{aligned} \tag{56}$$

$$\begin{aligned}Nu_2 &= 0{\cdot}156, \\ Nu &= 0{\cdot}07156\theta^{-\frac{1}{2}}\sqrt{(Re)}+0{\cdot}156, \\ Nu/Nu_1 &= 1+2{\cdot}19\theta^{\frac{1}{2}}/\sqrt{Re},\end{aligned} \tag{57}$$

for the convex circular surface, and

$$\begin{aligned}C_{f_2} &= (0{\cdot}905+0{\cdot}0900\theta)\theta^{-\frac{1}{2}}/Re, \\ C_f &= \theta^{-\frac{1}{2}}/(36\sqrt{Re})+(0{\cdot}905+0{\cdot}0900\theta)\theta^{-\frac{1}{2}}/Re, \\ C_f/C_{f_1} &= 1+(32{\cdot}59+3{\cdot}24\theta)\theta^{-\frac{1}{2}}/\sqrt{Re},\end{aligned} \tag{58}$$

$$\begin{aligned}Nu_2 &= -0{\cdot}168, \\ Nu &= 0{\cdot}07156\theta^{-\frac{1}{2}}\sqrt{(Re)}-0{\cdot}168, \\ Nu/Nu_1 &= 1-2{\cdot}35\theta^{\frac{1}{2}}/\sqrt{Re},\end{aligned} \tag{59}$$

for the concave circular surface. It is seen from the foregoing equations that the second-order term has a much greater effect on the friction factor than on the Nusselt number.

Consideration may now be given to the determination of the reference velocity $\bar{u}_r$ and the effective origin of the wall jet. The need to determine the latter arises because the conditions at $\theta = 0$ which

emerge from the analytical solutions are rarely encountered at the point of origination of an actual wall jet.

It is interesting to recount the approach employed in prior wall jet analyses to fix the reference velocity (no attempt was made to determine the effective origin). In recognition of the fact that the total momentum is not conserved in a wall jet owing to friction at the bounding wall, Glauert [1] defined another quantity which he called the flux of exterior momentum. This quantity is an invariant for the plane wall jet and, therefore, it was used by Glauert to eliminate the reference velocity. On the other hand, it is not an invariant for curved wall jets in the Reynolds number range where the flow is expected to be laminar. For instance, for a Reynolds number of 1000, the deviation from constancy is about 100 per cent for a parabolic wall jet according to Clark and Watson [6]. At high Reynolds numbers, the deviation is much smaller (e.g. 10 per cent for the Clark–Watson case at $Re = 10^5$), but the flow is not expected to be laminar.

In the present problem, it is possible to deduce both the effective origin of the wall jet and the unknown reference velocity which determines the Reynolds number by comparing analysis and experiment. Inasmuch as Nu_2 has been found to be a universal constant (independent of Re and θ) at a fixed Prandtl number, equation (49) can be rewritten as

$$\{\tfrac{1}{4}t_1'(0)\sqrt{Re}/(Nu-Nu_2)\}^{\frac{4}{3}} = \theta. \qquad (60)$$

With Nu_2 from analysis and data for Nu vs θ from experiment, $(Nu-Nu_2)^{-\frac{4}{3}}$ can be plotted as a function of θ. The extrapolation of the resulting straight line provides an intersection with the θ axis. The value of θ at the intersection point is the effective origin of the wall jet. Furthermore, from the slope of the line and the known value of $t_1'(0)$, the Reynolds number (and, hence, the reference velocity) is determined.

CONCLUDING REMARKS

The flow and heat transfer in a laminar wall jet on concave and convex circular surfaces has been solved using Van Dyke's technique of inner and outer expansions. The heat-transfer results were obtained for $Pr = 0{\cdot}72$. The local friction factor corresponding to the first-order equations was found by Glauert and is given by equation (21); the associated local Nusselt number is readily calculated by solving the energy equation and is expressed by equation (44). The effects of curvature and displacement are represented by the second-order equations. The second-order correction increases the friction factor and is larger for the concave surface than for the convex surface. On the other hand, the second-order correction either increases or decreases the Nusselt number depending on whether the surface is convex or concave; this correction is independent of θ. Approximate representations for the local friction factor and Nusselt number are expressed by equations (56)–(59).

The Coanda Effect, whereby an induced pressure deficit presses the flow against a curved surface, was demonstrated by the analysis. A technique for determining the effective origin of the wall jet flow and the reference velocity (and Reynolds number) was proposed.

REFERENCES

1. M. B. Glauert, The wall jet, *J. Fluid Mech.* **1**, 625–643 (1956).
2. A. Plotkin, A second-order correction to the Glauert wall jet solution, *AIAA Jl* **8**, 188–189 (1970).
3. I. J. Wygnanski and F. H. Champagne, The laminar wall-jet over a curved surface, *J. Fluid Mech.* **31**, 459–465 (1968).
4. B. Lindow and I. Greber, Similarity solution for a laminar, incompressible jet flowing along a curved surface, *AIAA Jl* **6**, 1331–1335 (1968).
5. A. Plotkin, The flow of a laminar, incompressible jet along a parabola, *J. Appl. Mech.* **39**, 13–17 (1972).
6. A. L. Clark and E. J. Watson, Displacement and curvature effects in a wall jet, *J. Fluid Mech.* **50**, 369–392 (1971).
7. M. Van Dyke, Higher approximations in boundary-layer theory, *J. Fluid Mech.* **14**, 161–177 (1962).
8. K. Gersten and J. F. Gross, Mass-transfer effects on higher-order boundary-layer solutions: the leading edge of a swept cylinder, *Int. J. Heat Mass Transfer* **16**, 65–79 (1973).

ECOULEMENT ET TRANSFERT THERMIQUE DANS DES JETS PARIETAUX INCURVES SUR DES SURFACES CIRCULAIRES

Résumé—On considère des jets pariétaux incurvés (c'est à dire, l'écoulement le long d'une paroi courbée dans la direction du mouvement) et, en particulier, des écoulements le long d'une surface circulaire convexe ou concave. L'écoulement laminaire et les caractéristiques du transfert thermique sont étudiés avec l'aide de la méthode des développements intérieurs et extérieurs. Les équations de Navier–Stokes et de l'énergie sont développées en séries, $1/\sqrt{Re}$ étant le paramètre du développement. Les équations du premier ordre sont identiques aux équations du second ordre représentent des corrections dûes aux effets de courbure et de déplacement. Ces dernières équations ont été résolues par une méthode de différences finies, avec $Pr = 0{,}72$ dans l'équation d'énergie. La correction du second ordre augmente le cisaillement à la paroi, l'augmentation étant plus grande pour l'écoulement sur une surface concave que pour l'écoulement sur une surface convexe. D'autre part, la correction du second ordre accroit ou diminue le nombre de Nusselt, suivant que la surface est convexe ou concave. L'effet Coanda, par lequel une différence de pression transversale induite empêche la séparation de l'écoulement, a été expliqué par l'analyse.

STRÖMUNG UND WÄRMEÜBERGANG IN GEKRÜMMTEN WANDSTRAHLEN AN KREISFÖRMIGEN OBERFLÄCHEN

Zusammenfassung—Es werden gekrümmte Wandstrahlen betrachtet (z.B. bei der Strömung entlang einer Wand, die in Strömungsrichtung gekrümmt ist) und insbesondere die Strömung an konvexen und konkaven kreisförmigen Oberflächen. Die laminare Strömung und die Charakteristik des Wärmeübergangs wird nach der Methode der sogenannten inneren und äußeren Expansion untersucht: Die Navier–Stokes- und die Energiegleichungen werden in Reihen entwickelt mit $1/\sqrt{Re}$ als dem Expansions-Parameter. Die Gleichungen erster Ordnung sind mit den konventionellen Grenzschichtgleichungen identisch, während die Gleichungen zweiter Ordnung Korrekturen für die Krümmung und Verdrängungseffekte liefern. Die letzteren Gleichungen wurden durch eine Differenzen-Differential-Methode gelöst mit $Pr = 0{,}72$ für die Energie-Gleichung. Die angegebene Korrektur wirkt hin zur Vergrößerung der Wandschubspannung, wobei die Vergrößerung für Strömungen über konkave Oberflächen größer ist als über konvexe. Andererseits wird die Nusselt–Zahl durch die Korrekturen entweder vergrößert oder verkleinert, wiederum abhängig von der Oberflächenkrümmung. Der Coanda-Effekt, bei dem eine induzierte Querdruck-Differenz zu einer Strömungsablösung führt, wurde in der Analysis demonstriert.

ТЕЧЕНИЕ И ТЕПЛООБМЕН В ИСКРИВЛЕННЫХ ПРИСТЕНОЧНЫХ СТРУЯХ НА КРУГЛЫХ ПОВЕРХНОСТЯХ

Аннотация — Рассматриваются искривленные пристенные струи (т. е. течение вдоль стенки, искривленной по направлению течения) и, в частности, обтекание выпуклой или вогнутой круглой поверхности. Методом внутренних и внешних разложений анализируются характеристики ламинарного течения и процесса теплообмена. Уравнение Навье–Стокса и уравнение энергии разлагаются в ряды, где в качестве параметра разложения взята величина $1/\sqrt{Re}$. Уравнения первого порядка идентичны обычным уравнениям пограничного слоя, в то время как уравнения второго порядка являются поправками на эффекты кривизны и смещения. Последние уравнения решаются разностно-дифференциальным методом. Для уравнения энергии значение числа Прандтля равно 0,72. Поправка второго порядка увеличивает значение напряжения на стенке, причем для вогнутой поверхности увеличение значительнее, чем для выпуклой. С другой стороны, поправка второго порядка или увеличивает, или уменьшает значение числа Нуссельта в зависимости от того, является ли поверхность выпуклой или вогнутой. С помощью данного анализа демонстрируется эффект Коанда, когда индуцированная поперечная разность давлений вызывает торможение срыва потока.